Molecular BioSystems

Accepted Manuscript

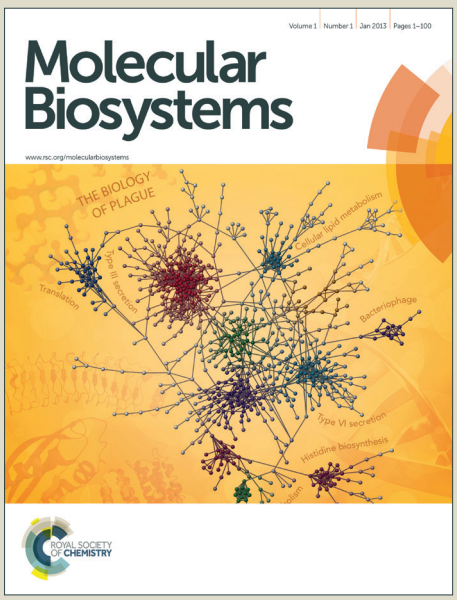

ROYAL SOCIETY OF CHEMISTRY

www.rsc.org/molecularbiosystems

Structural Elucidation of SrtA enzyme in *Enterococcus faecalis:* An Emphasis *on* Screening of Potential Inhibitors against the Biofilm Formation

Chandrabose Selvaraj[1], Jeyachandran Sivakamavalli[2], Baskaralingam Vaseeharan[2], Poonam Singh[3] and Sanjeev Kumar Singh[1]*

[1]Computer Aided Drug Design and Molecular Modeling Lab, Department of Bioinformatics, Alagappa University, Karaikudi-630 004, Tamil Nadu, India

[2]Crustacean Molecular Biology & Genomics Lab, Department of Animal Health and Management, Alagappa University, Karaikudi-630 004, Tamil Nadu, India

[3] Toxicology Division, Central Drug Research Institute, Lucknow -226 001, Uttar Pradesh, India

Correspondence and reprint requests to:

Dr. Sanjeev Kumar Singh, Ph.D,
Associate Professor,
Computer Aided Drug Design and Molecular Modeling Lab,
Department of Bioinformatics,
Alagappa University, Karaikudi-630003,
Tamil Nadu, India,
Phone: +91 4565 230725, Fax: +91 4565 225202
E. Mail: skysanjeev@gmail.com

Short title: Targeting signal transduction mechanism in *Enterococcus faecalis*

Table of contents entry

SrtA enzyme is associated with microbial surface proteins embedded signal transduction mechanism. Present work is an inclusive report of structural elucidation in SrtA from *E. faecalis* through computational and experimental methodologies.

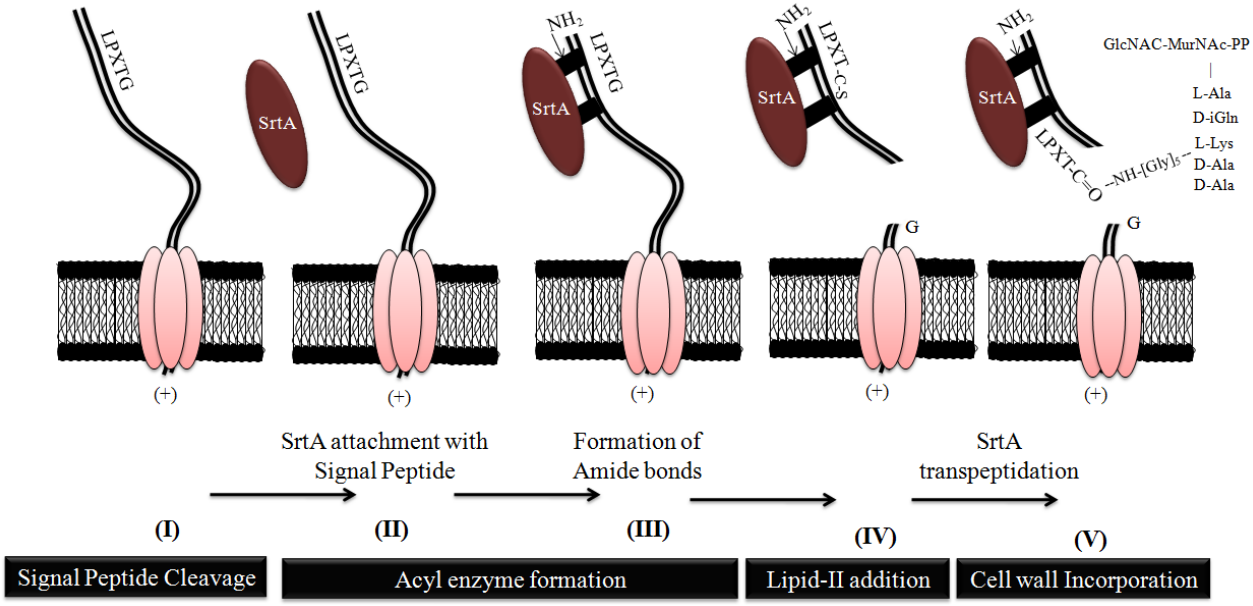

Abstract

Enterococcus faecalis is a pathogenic, Gram-positive bacterium which mainly infects humans through urinary tract infections. SrtA is an essential enzyme for survival of *E. faecalis*, and inhibition of this particular enzyme will reduce the virulence of biofilm formations. It is proved to be associated with microbial surface proteins embedded signal transduction mechanism and promising as a suitable anti-microbial drug target dealing with *E. faecalis*. In this present work is an inclusive description of SrtA from *E. faecalis* through computational and experimental methodologies. For exploring the mechanism of SrtA and to screen potential leads against *E. faecalis*, we have generated three-dimensional models through homology modeling. The 3D model showed conformational stability over time, confirming the quality of the starting 3D model. Large scale dynamics of 100ns provide the event of intramolecular changes occurs in the SrtA, and multiple conformation of structure based screening elucidate potential leads against this pathogen. Screened compounds are experimentally active by showing anti-microbial and anti-biofilm activity, even as SrtA is known to play an important role in *E. faecalis* biofilm formation. Outcome of experimental activity suggest that, SrtA specific screened compounds have better anti-biofilm activity than the available inhibitors. Therefore, we believe that development of these compounds would be an impetus to design the novel chief SrtA inhibitors against *E. faecalis.*

Key words: Anti microbial; Anti Biofilm; CLSM; Homology Modeling, Molecular Dynamics, SEM; SrtA

Introduction

Enterococcus faecalis is an immobile, low-GC; Gram-positive spherical bacterium that causes a variety of nosocomial infections in which urinary tract infections are the most commonly caused diseases in humans[1-2]. It is commonly found in diverse environments including food, water, soil and plants, but it's also associated with life-threatening infections. These organisms are present in single, pairs or in short chains and it have the characteristics features of colony forming unit. It is a facultative anaerobe with a fermentative metabolism and is mostly located in the large intestine of humans[3-4]. *E. faecalis* ranks among the leading causes of hospital acquired bacterial infections thus causing mostly urinary tract and intra-abdominal infections, infective endocarditis and bacteremia [5]. The infections caused by *E. faecalis* are difficult to treat because of their recurrent resistance to multiple antibiotics including vancomycin, a drug considered to be a last resort for many Gram-positive infections[6-8]. Therefore it has become necessity to find a new metabolic target that are essential for bacterial survival and proliferation within its host in order to strategically develop new and efficient drugs against *E. faecalis.* Generally protein anchoring to the cell wall is a conserved mechanism of Gram-positive bacteria for the display of proteins in an envelope devoid of an outer lipid bilayer. Cell wall anchored proteins **carries** two topogenic signals, one for translocation across the membrane and another one for recognition by transpeptidase enzyme, designated sortases. Surface proteins are key factors for understanding the behavior of Gram-positive bacteria interacting with the human gastro-intestinal tract.

Such proteins contribute to cell wall synthesis, keeping patterns and also important for interactions between the bacterial cell and the human host[9]. Since they are exposed and may play roles in pathogenicity, surface proteins are interesting targets for drug design. Especially the

amino acids Leucine, Proline, X, Threonine, and Glycine (LPXTG, where X denotes any amino acid) involved surface proteins plays the vital role in pathogenicity in Gram positive bacterium. Researchers have been trying to inhibit the bacterial surface proteins which are responsible for the biofilm production and cell adhesion mechanism [10]. In *E. faecalis*, a well known housekeeping gene sortase A (SrtA) is responsible for the biofilm formation and virulence in catheter associated urinary tract infections (CAUTIs) [11-12]. Previously the vital role of autolysin (Atn), eDNA, and SrtA were reported in *E. faecalis* during the developmental stages of biofilm formation under static and hydrodynamic conditions [13].

The SrtA structure captures the recognition signal consists of the LPXTG motif and cleavage occurs between the Thr and Gly, with transient attachment through the Thr residue to the active site Cys residue, followed by transpeptidation that attaches the protein covalently to the cell wall[14]. **(Figure 1)** The above mentioned figure explains the cell wall assimilation through SrtA mechanism, which generally includes signal peptide cleavage, formation of amide bonds, acyl enzyme formation and lipid II addition leads to incorporation of bacterial cell wall. This mechanism is much important in bacteria, especially in cell adhesion, host-bacteria interactions and in biofilm formations. Formerly, the role of sortase gene (SrtA) in monospecies biofilm formation was investigated in *Streptococcus mutans* and it was observed that inactivation of SrtA caused a decrease in biofilm formation[15]. The same mechanism of biofilm inhibition is also reported in *Staphylococcus aureus, S. agalactiae, S. gordonii, Bacillus cereus etc*[16-18]. The reported literatures on SrtA clearly explain that, deactivation or inhibition of SrtA appears to be dramatically reducing the biofilm growth pattern [19]. *E. faecalis* biofilm architecture contains numerous protective features including extracellular polysaccharide matrix that render biofilms impermeable to conventional antimicrobial agents [20-21.] The biofilms are defined as communities

of microorganisms attached to a surface and consist of a population of cells attached irreversibly on various biotic and abiotic surfaces, encased in a hydrated matrix of exopolymeric substances. It is clear that microorganisms undergo profound changes during their transition from planktonic (free-swimming) organisms to cells that are part of a complex, surface-attached community [22-25]. To control or inhibit the biofilm formation in *E. faecalis*, the protein SrtA mechanism of signal transduction has to be terminated [26].Hence, the present study is focused on the cell surface protein SrtA inhibition through computational modeling and screening of drugs with the ability of antimicrobial and anti biofilm activity. The crystal structure of SrtA from *E. faecalis* has not yet been solved through X-ray *crystallography*; therefore we have constructed the 3D models of SrtA from *E. faecalis* and screened the potential inhibitors against the biofilm formation.

Materials and Methods

Theoretical platform: All the theoretical works were carried out on a High Performance Cluster operated with Cent OS V5.5 Linux operating platform. Hardware specifications of HPC cluster-Super micro SC826TQ-R1200 LIB series, running with 2 ATOM processor of 32 Core and 32 GB RAM speed. Software specifications used for MD simulation run and molecular modeling studies are academic version of GromacsV.4.5 molecular dynamics package [27] and commercial version of Schrodinger software package, LLC, New York, NY 2012 [28] respectively.

Experimental platform: The experimental works were carried out with quality control strain of *E. faecalis* (ATCC No. ATCC35550). For this study, the strain is cultured aerobically and maintained in Luria–Bertani (LB) broth (Himedia, India) at their optimum temperature of 37□C under 150 rev/min. The screened compounds are obtained from (SIGMA, USA) and (Hi-Media,

Mumbai, India) were used for the experimental purpose. Details of the screened compounds ID is provided separately as supplementary information.

Template search and sequence alignment

The sequence of SrtA enzyme from *E. faecalis* was retrieved from NCBI sequence database (WP_010715428). A BLASTP search was performed with default parameter against the Brook Heaven Protein Data Bank (PDB) in finding appropriate template structure for circumventing the homology modeling. [29] The criterion is to take up high percentage of sequence identity and lower e-value structures as template. Based on this criterion, the PDB ID -2KW8 (SrtA from *B. anthracis*) with 34% identity was chosen as an appropriate template. Even though, the identity between target and template was comparatively low, the functions of both the sequences were found to be unique and so the template 2KW8 is chosen to be the suitable template. The alignment between target and template sequence was carried out using ClustalW [30]. The secondary structure is predicted using STRIDE: a tool for secondary structure assignment from atomic resolution protein structures [31]. It utilizes empirically derived hydrogen bond energy and phi-psi torsion angles to assign secondary structure. Secondary structure with its subsequent sequence alignment was viewed through Espript [32].

Homology Modeling and Validation

The 3D structure of SrtA from *E. faecalis* was not found in PDB entry with the present exercise of developing the quality 3D model has been undertaken**.** The coordinate file of template 2KW8 structure was retrieved from the PDB while the homology modeling was performed by using modeller9v10 [33]. The model protein structures were ranked based on the internal scoring function (DOPE score), and models with least internal score were identified and subjected to model

validation. Before running the MD simulation, the coordinates of predicted refined model was checked for dihedral angle distribution using Ramachandran plot in the PROCHECK [34]. The ProSA tool used to check the overall modeled protein structure for potential errors. The root mean square deviation (RMSD) between the main chain atom of the model and the template was calculated by superimposing the structure of the template on the predicted structure of SrtA enzyme protein in order to assess the reliability of the model using chimera Matchmaker tool [35].

Molecular Dynamics Simulation

The MD simulation study is executed for the homology modeled SrtA structure of *E. faecalis* for 100ns of timescale, in order to understand the stability and intra-molecular conformational changes occurs in the protein structure. The GROMACS program package [26] adopting the OPLS-AA force field parameters are used for energy minimization and MD simulations. For the MD simulation studies, the structure is solvated in the TIP3P water model, and energy minimized using steepest descent method, terminating when maximum force is found smaller than 100 KJ mol^{-1} nm^{-1} [36]. The structure is minimized till least energy conformation to eliminate bad atomic contacts. The total simulation are performed in the NPT ensemble at constant temperature (300 K) and pressure (1 bar), with a time step of 2fs. NVT (constant Number of particles, Volume, and Temperature) and "canonical" ensemble is performed for 1ns, and the minimized structure is equilibrated with a timescale of 100ns [37]. Additionally, the MD simulations are also performed for the ligand bound docked structures of SrtA which are the outcome of high throughput virtual screening. The initial structure of the receptor and ligands were cleaned using OPLS-AA force field and then the topology files are generated for the receptor and ligands separately using PRODRG tool [38]. The simulation system was thus created manually by importing the ligand

topology into the system pursued along with a dodecahedron box with a margin of 1nm. The system was later filled with water using the TIP3P explicit solvation model and then applied with energy minimization and the atomic velocities were adjusted according to Maxwell Boltzmann distribution at 300K with a periodic scaling of 0.1ps. A presimulation run of 20ps was applied to relax the system and to remove the geometric restrains which eventually appeared at the initialization of the run. All the simulations were carried out at constant pressure and temperature (NPT) ensemble. The Berendsen coupling is employed to maintain a constant temperature of 300K and constant semi-isotropic pressure of 1 bar with coupling time of 2.0fs and the coordinates are saved**.** The simulation timescale for ligand bound form was set at 20ns and the RMSD (Root-Mean-Square-Deviation), hydrogen bond analysis was performed to understand the stability of ligands [39-40].

Active site prediction

The modeled SrtA refinement process is performed through Protein preparation wizard before using in Schrodinger molecular modeling platform**.** Because the homology model protein has neutral charges, which is not compact for docking and other molecular modeling techniques. So that, the protein preparation wizard implemented by Schrödinger to check for missing information on connectivity, which must be assigned along with bond orders and formal partial charges. During the preparation bond order of residues were assigned even as addition of hydrogen atoms and also hydrogen bonding network was optimized. The optimized model structure was minimized until the average RMSD of the non-hydrogen atoms reached 0.30Å using the OPLS-AA force field [41]. The modeled structure binding site information has not yet been reported; hence we hope that the prediction of these binding site regions will enhance the

new leads discovery. Here the possible binding sites were predicted based on druggability region through sitemap with OPLS-2005 [42-43]. The druggability regions were identified by various physical descriptors like size, degree of enclosure, degree of exposure, tightness, hydrophobic, hydrophilic, hydrogen bonding possibilities, and linking site points which were more likely to be contributing to protein-ligand binding.

High Throughput Virtual Screening

The complete Drug bank database of total, six thousand eight hundred and twenty five compounds are prepared by using 'LigPrep 2.5' module. Optimized Potential for Liquid simulation (OPLS)-2005 force field is applied to retain original state and chirality of ligands. In order to avoid strange conformation of complex structure, the lead compounds that retained original state were manually picked [44]. Structure-based virtual screening was performed in the Virtual Screening Workflow (VSW), to identify potential ligand molecules that interact with druggability regions of the SrtA structure. The average conformation of the SrtA structure from the MD simulation was taken for the docking studies. The screened compounds were docked through filtering criteria of HTVS, SP and XP docking [45]. After ensuring the suitability of protein and ligand for docking, the receptor grid file is generated using a grid-receptor generation program. To soften the potential for non-polar part of receptor, we scaled Van der Waal radii of receptor atoms by 1.0Å with a partial charge cutoff 0.25 [46].The docking based screening protocol includes three different phase and in each phase, the best compounds are chosen for next phase based on its scoring values. The compounds with less scoring values were eliminated at each docking phase and better scoring hit compounds are passed in each docking phase [47]. Glide XP mode determines all reasonable conformations for each low energy conformer in the designated binding site. In this process, the torsional degrees of each ligand were relaxed, though the protein

conformation was fixed. During the docking process, the Glide scoring function (G-score) was used to select the best conformation for each ligand. The final energy evaluation was done with Glide score and a single best pose is generated as output for a particular ligand[43, 46].

Induced Fit Docking

Although screening is performed with the rigid receptor and flexible ligand molecules, here we endeavour different flexible conformations of protein by using Induced Fit Docking (IFD) approach[48-50]. The SrtA active site architecture of a protein has flexible loops and it depends heavily upon conformational changes induced by the bound ligand. Through Induced fit docking, possible binding modes and the associated conformational changes within receptor active sites are analyzed through multiple docking conformations. Including multiple receptor conformations based IFD technique in virtual screening methods allow the ligand in the binding pocket and guide the conformational changes of the receptor without changing the backbone structure of protein. Rigid receptor cordially estimates ligands within binding site and scoring functions will provide conformations based on its interactions. But both protein and ligand in flexible condition, with multiple protein conformations will provides the maximum possibility of accurate interactions [51]. This is laid possibility of combined protocol of prime and Glide through IF-Docking. The final best 10 compounds on VSW screening were further refined through IFD. Here, each docked conformers in previous step was subjected to side-chain and backbone refinements through prime. Different possible conformations are generated through prime and multiple conformations are docked through glide. The refined complexes were ranked by prime energy, and the receptor structures within -30 kcal/mol of the minimum energy structure were passed for a final round of Glide docking and scoring [52]. The side chain orientations have been

performed automatically with inclusion of prime in IFD. An IFD score that accounts for a calculation of both the protein–ligand interaction energy and the total energy of the system [41].

Free energy Calculation

The binding calculation done through prime-MM/GBSA (Molecular Mechanics/Generalized Born Surface Area) is physically more rigorous than docking [53]. Prime uses a surface GB model employing a Gaussian surface instead of a Vander Waals surface for better representation of the solvent accessible surface area [54]. Binding energy was calculated by the following equations,

$$\Delta G_{bind} = \Delta_E + \Delta G_{solv} + \Delta G_{SA} \quad (1)$$

$$\Delta_E = E_{complex} - E_{protein} - E_{ligand} \quad (2)$$

Where, $E_{complex}$, $E_{protein}$, and E_{ligand} are the minimized energies of the protein-inhibitor complex, protein, and inhibitor, respectively [55]

$$\Delta G_{solv} = G_{solv}(complex) - G_{solv}(protein) - G_{solv}(ligand) \quad (3)$$

Where, G_{solv}(complex), $G_{solv(}$protein), and G_{solv}(ligand) are the solvation free energies of the complex, protein, and inhibitor, respectively.

$$\Delta G_{SA} = G_{SA}\ (complex) - G_{SA}\ (protein) - G_{SA}\ (ligand) \quad (4)$$

Where, G_{SA} (complex), G_{SA} (protein), and G_{SA} (ligand) are the surface area energies for the complex, protein, and inhibitor, respectively [56]. The rational criteria for selection of best compounds based on scoring and interaction parameters shown in XP docking and IFD docking are forwarded to MD simulation studies and experimental validation.

In vitro* anti-microbial activity of screened compounds against *E. faecalis

The structure based screen compounds were validated through *in vitro* anti-microbial activity against *E. faecalis.* The disc diffusion test was performed in Muller Hinton Agar (MHA) (Himedia Laboratories, India). Overnight cultures of the *E. faecalis* were sub-cultured until a turbidity of 0.5 McFarland (1×106 CFU/ml) was reached. Using a sterile cotton swab the culture was uniformly spread over the surface of the agar plate. Absorption of excess moisture was allowed to occur for 10 min. Then 0.5–12 μg/ml of the screened compounds was loaded onto the wells. Further, the MHA plates were incubated at 37 °C and the zone of inhibition is measured after 24 h. The Minimal Inhibitory Concentration (MIC) of the screened compounds was performed as per CLSI 2006 guidelines. The bacterial suspension 10^6 CFU/ml are added with the screened compounds serially diluted two fold to give final concentrations ranging from 0.5 to 2000 μg/ml and incubated at 37 °C for 24 h. The MIC was recorded as the lowest concentration that produced inhibition of visible growth after overnight incubation. The diameter of the inhibition zone was measured and noted as anti-microbial activity values. The MIC of the screened compounds is examined using 10^6 Colony Forming Units (CFU) for Gram positive *E. faecalis* on LB agar plates (in triplicates). Different concentrations of screened compounds (5, 10, 15, 20, and 25 μg/ml) are inoculated and tested against the pathogen. The plates with screened compounds along with control are incubated for 24 h at 37 °C and the numbers of colonies were counted.

Growth curve Kinetics

Bacterial growth kinetics in the presence of screened compounds and control are monitored by inoculating in the microtiter plate wells with nutrient broth containing 10^7 CFU/ml and loaded with different concentrations of drug (0.1–5 mg/ml). The plates were incubated at 37 °C, 100 rpm and the absorbance was recorded at 600 nm for 24 hrs.

Biofilm formation and biofilm inhibitory concentration (BIC)

The Biofilm inhibitory concentration (BIC) is determined as the lowest concentration of screened compounds which have the potential for visible inhibition of the biofilm formation and leads to significant reduction in the biofilm growth in compare to the control wells exactly reading at $OD_{570nm.}$ The screened compounds with the concentration ranging from 30-40 µg/ml were then added into the bacterial suspension of 10^6 CFU/ml [57]. The plates containing glass pieces were incubated for 24- 72 h at 37 °C. The glass pieces were stained with 0.04% crystal violet and the sub inhibitory concentration (0.5 and 0.25 BIC) of the screened compounds was also tested against biofilm formation by performing the same protocol. Subsequently, the determination of BIC and the Sub-BIC were performed using spectro photometric quantification.

***In situ* visualization analysis**

a, Light Microscopy: For microscopic analysis, bacterial culture 10^7 CFU containing bacteria was transferred into each well of a 24-well polystyrene microtiter plate (Corning) in which sterile glass pieces had already been placed. The bacterial biofilm plates incubated for 48 to 72 h were further treated with the screened compounds and crystal violet (CV) staining is performed for the grown biofilm (200µl of 0. 2% CV staining solution (w/v)) for 10 min and allowed to dry before solubilization of the staining reagent with 1ml of absolute ethanol. After performing the staining, the stained glass pieces were placed on slides with the biofilm pointing up and inspected at magnification of 40X. Visible biofilms were viewed by light microscopy documented with an attached digital camera (Nikon, Eclipse, Ti 100).

b, Confocal laser scanning microscopy (CLSM):

In CLSM analysis, biofilms of various bacterial strains were allowed to form on the biofilms as described in light microscopic analysis. After 24-72 h, biofilm formed in glass slides were stained with 20 µl of 0.1% acridine orange (Sigma Aldrich, Switzerland). The excess stain was washed out and the stained cover glasses were visualized with CLSM (LSM 710, Carl Zeiss, Germany) equipped with an excitation filter 515–560 and magnification at 20x.

c, **Scanning electron microscopy (SEM):** For SEM analysis, biofilms containing glass pieces were fixed for 1 h in a 2.5% glutaraldehyde. The glass pieces were washed in 0.1M sodium acetate buffer (pH 7.3). Samples were subsequently washed in distilled water, dehydrated in a series of ethanol washing (70% for 10 min, 95% for 10 min and 100% for 20 min), dried, gold sputtered and examined with a Hitachi S-3000H (Japan).

3. Results and Discussion

3.1. Sequence alignment and Secondary Structure Prediction

The main criterion in homology modeling is choosing the appropriate template and sequence alignment between the target and template. BLASTp result provided the sequence identity between the target protein (SrtA) and the template 2KW8 is 34%. In addition to this, the sequence alignment was performed to align the target protein sequence (SrtA) with the template protein sequence (PDB ID: 2KW8) using ClustalW program (**Figure 2**). The amino acids from 26-43, 50-75 and 130-154 were found to be more conserved between the template and target sequence. Secondary structure prediction technique is aimed to predict the local secondary structure of proteins in their amino acid sequences such as alpha helices, beta strands or coils. The Espript web server, written in the python programming language was implemented for assigning the secondary structure elements of SrtA protein sequence. Secondary structure

prediction of modeled protein comprises of high beta-sheet and overall holds eight beta sheets, one alpha-helix and four eta-sheets. The alignment of template and target with its secondary structures are provided in the **Figures 2 and S3** respectively.

Homology modeling and Validation

Homology modeling performed on best hits from blastp searches yielded 2KW8 (NMR structure of SrtA from *B. anthracis*) with 34% identity which also has similar functional role of SrtA in different bacteria. Default template structure is obtained from NMR structure of *B. anthracis* SrtA, which showing -6.41kcal/mol Z-score is separated from NMR structure and used as template structure for the homology modeling. Based on this template, ten models were predicted based on its function of their energy, and the best model structure was identified by their respective dope score. The model having minimum dope score was considered as the best model of the protein and considered for further evaluation (**Table S1; Figure 3A**). To evaluate the quality of predicted model, the least energy model is subjected for several validations. The results recommend the obtained model is perfect, in terms of the main-chain stereochemistry and amino acid environment. In the Ramachandran plot (**Figure S1**), 83.2 % of the residues were found to be in the fully present in the allowed region while 12.4% in additionally allowed region, 2.9% in generously allowed region and 1.5% residues in disallowed region. These model validation results point out the backbone dihedral angles of ψ and φ angles in the model are reasonably accurate. Additionally, PROSA server is used to check potential errors in predicted 3D models of protein. The Z-score indicated the overall quality of model and also measure the deviation of total energy in predicted model with respect to energy distribution from random conformations. The Z-score of the template is -6.41kcal/mol and of target is -6.86kcal/mol (**Figure S2**) and it indicates that the modeled structure is much similar to template structure. The

accurate model must have the RMSD value less than 2Å while the calculated root mean square deviation between the target and template was found to be RMSD = 0.28Å using chimera (**Figure 3B**). From these results, the predicted model is more reliable and accurate, based on stereo chemical and overall quality factors. The final refined model is subjected for other molecular modeling calculations.

Conformation analysis for protein backbone

In MD simulation, the C-α of protein model was analyzed to understand the stability in solvent environment. The RMSD assessments of C-α atoms from MD simulation are plotted with respect to time-dependent function. The entire simulation results support the model protein by showing constant RMSD deviation while the model structure in MD simulation here is shown as an evidence for stable along with the intention of lively response in dynamic movement. The overall simulation process is a large scale 100ns timescale and represent up and down deviations in RMSD plot. Deviations are slightly irregular up to 60ns and secondary structure elements of loops structures present in the modeled SrtA are showing many fluctuations than the other secondary structures (**Figure 4a**). Figure 4a, explains the total average deviations of SrtA structure for the 100ns of timescale and in focus of attaining the stable position has been zoomed. The quality of average structure is visualized and compared with initial model structure and it shows model protein structure is refined based on molecular dynamics simulations. The initial and average protein structure is showing the RMSD variation of 0.82Å and this particular conformation are used for the molecular modeling studies. The deviations in position of the average conformations are relatively same, which explains the architecture of the protein relatively similar after simulation. Lively conformations are holding more active pattern in

between 40-60ns and stability is viewed after 60th ns by attaining the equilibrium constant. The modeled structure has more loop structures with its protein architecture and fluctuating loops are shown in the **Figure 4b**. RMSF plot clearly shows that the fluctuations are seen only in loop regions and is not overlapping with the other structural proximities and secondary structural elements. The water solvent present in boundary box had very good interaction with modeled protein and this is the reason behind stability of the protein near to its original position **(Figure 4C)**. The interaction between water model and protein is calculated and it showing the average of 1557 H-bonds within 0.35nm and 314 H-bonds above 0.35nm distance. The MD simulation presents several conformations with respect to time scale event and from that, the average stable structure was chosen for the molecular modeling calculations.

Virtual screening for SrtA: Glide and IFD approach

The drug bank database set is well prepared using ligand preparation and used for the virtual screening of suitable hit compounds against the SrtA from *E. faecalis*. Entire drug bank database of total 6825 five compounds are docked with predicted active site of SrtA structure. Predicted active site region shows Ser1, Leu2, Ala3, Gln5, Arg7, Pro8, Asp46, Ser47, MET117, THR118, THR120, Ile134, THR135, GLN138, lys141, and ARG145 amino acids can function as druggability amino acids (Supplementary figure S4). These amino acids required new and specific compounds to be adopted and inhibit the function of SrtA. The combined approach of VSW and IFD was implemented for the identification of appropriate compounds against the SrtA. Our approach was executed with four stage of docking and at each stage of docking, we believe would eliminate the in apt compounds based on scoring. While VSW provided HTVS, SP and XP docking, the XP docking could be considered the final stage, which holds only appropriate compounds based on Gscore. Here, only the compounds able to catch up the

environment of predicted druggability pockets were held while all other compounds were eliminated. Even though the drug bank database has several thousand compounds only fifteen compounds were ahead of VSW. Glide based VSW applied the flexible docking algorithm and here the flexibility is restricted towards ligand atoms only. In IFD docking, both the ligand and proteins are flexible and the algorithm applies combination of protein modeling, simulation and docking. Binding pocket fit approach deals with multiple conformation of protein and hit compounds on VSW were redocked. This approach combines in an iterative fashion of ligand docking techniques with those for modeling receptor conformational changes. Results of IFD are illustrated in the table 1 (best 5 compounds), which clearly shows that all the screened compounds are more affinity towards the binding of SrtA. Most commonly, the amino acid residues of SER1, LEU2, GLU4, GLY5, CYS136, LYS141 and ARG145 are commonly involving in interaction with hit compounds. The best five compounds namely Amoxicillin, Cefixime, Esomeprazole, Cephalexin, and Losartan are showing better scoring and interactions. From all these compounds, Losartan is showing comparatively low energetics towards SrtA. Esomeprazole and Losartan show three hydrogen bond interaction and other three compounds are showing very good interactions with the SrtA binding site amino acids. The distance between the protein ligand interactions was found to be satisfactory by showing in standard level distance of 1.6-2.4Å. The Amoxicillin, Cefixime and Cephalexin compounds has more than five hydrogen bonds for interaction and the IFD score was found to be -331.10, -330.94 and -328.72 respectively. The Esomeprazole and Losartan ligands showed only three H-bonds that interacts with the receptor and the IFD score was -330.05 and -327.54 respectively. The docking energy between receptor and ligand showed that -50kcal/mol for Amoxicillin, Cefixime, Esomeprazole and Cephalexin. In case of Losartan, the docking energy is comparatively less and showing -

48.38Kcal/mol. The funnel based combined approach provides valid compounds based on both rigid and flexible receptor, and more over the best compounds are having better scoring and interaction factors [58]. The top 5 compounds based on scoring and interaction parameters shown in XP docking and IFD docking are forwarded to MD simulation studies and experimental validation.

Binding energy calculation

The IFD posture is minimized through local optimization feature in Prime, and the complex energies are calculated by using the OPLS-AA force field and GBSA continuum solvent model. The composite scoring method was applied for ranking the protein and ligand, accounting for the interaction energy and binding energy of docked complex. In the induced fit calculations, improvements of ranking in screened compounds were achieved by including the ligand – receptor solvation energy. The energy values obtained through IFD are represented in Table 1. Here Amoxicillin, Cefixime, Esomeprazole and Cephalexin are having better binding energy and these are due to strong bonding interactions occur between protein and ligand. These binding energies are having much correlation with docking energy and so the best compounds on this screening approach results with better binding energy.

Ligand Complex Simulation

The screened compounds are analyzed for its stability and interaction behavior through molecular dynamics simulation. Based on scoring values of docking and binding energy claculations, four best ligands were chosen for dynamic behavior studies, which were analyzed in trajectories. A molecular dynamics simulation shows that all the compounds on this dynamic event having better interactions throughout the timescale of 20ns and ligand does not disengage from the protein binding pocket. The **Figure 6a** shows the RMSD graph of top four active

compounds and these compounds are more stable inside the binding pocket due to the interactions with protein and ligands. The RMSD figure shows that initially all the compounds is slightly moved from its original position and after the binding of ligand position got stable inside the binding pocket and the bonding interactions holds the ligand strongly by not allowing the ligands to detach from the protein structure. From all the four compounds, except Amoxillin all the compounds are shown to be much stable (**Figure 6a).** RMSD values of particular compounds without its proteins structure inform that all the four compounds are much stable. The **Figure 6b**, explains the RMSD plot having stable frequencies of ligand molecules in the timescale of 20ns. Additionally, the ligand atoms are seems to be more active and generating more conformations in the dynamic point is found to be feasible. The values of RMSD with compare to movement of the proteins were due the flexible loops present in the modeled structures. Crystal structures of SrtA from *Staphylococcus aureus* and *Bacillus anthracis* are already reported to have more loop regions. Similarly, the modeled structure of *E. faecalis* also having the flexible loops regions in its secondary structure morphology. These loops regions are playing the vital role in the binding site allocations and ligand binding these regions will have comparatively more movements. The fluctuations of ligand-protein and ligand are represented in the **Figure 6c and 6d**, which shows the amino acids in the binding site regions, are comparatively fluctuated. From the Figure 6D, it clearly depicts the atomic fluctuations in the ligands and the ligand are more active inside the binding site pocket. The holding of screened compounds within the binding pocket of SrtA is made by the bonding interactions between the protein and ligand. Here, we checked the hydrogen bond analysis of protein and ligand contacts throughout the simulations. We perceive that the screened compounds have high potential towards the acceptor-donor relations and so there is a strong relation between protein and ligand. These acceptor-donor relation results with

hydrogen bond interactions throughout the 20ns of timescale. All the screened compounds showed the better bonding interactions with the average of 4 hydrogen bonds in each step (**Figure 6e).** These results suggest that binding of the ligand to the protein showed deviation from their initial position because of adjustments in their configuration but remains bound within the catalytic triad of the protein. Overall, the stable interaction pattern of ligand complex with SrtA is visualized in MD simulation studies and these compounds are validated by experimental techniques.

Antimicrobial susceptibility testing for computationally screened drugs

The antimicrobial activity of screened drugs were loaded with the different concentrations (5- 25 µg/ml) and the antimicrobial activity was tested against a Gram positive *E. faecalis* was determined (Table 3). Based on the *in silico* screening we have scrutinized the ten drugs for the antimicrobial assay. The mean value of five replicates and its zone of inhibition for each concentration for the best four drugs were determined to be about 17.3 ± 0.53 µg/ml, 16 ± 0.46 µg/ml, 15.8 ± 0.26 µg/ml, and 8 ± 0.7 µg/ml for Esomeprazole, Amoxicillin, Cephalexin and Cefaxime respectively. The highest antimicrobial activity was observed against Esomeprazole, whereas a lower activity was found at the concentration of Amoxicillin and very less antimicrobial activity was observed at Losartran. Minimum inhibitory concentration (MIC) results showed the least concentration of the drug control the *E. faecalis* activity. In this, colonies were grown on Luria–Bertani plates which were incorporated with different concentrations of Esomeprazole and 10^4 CFU *E. faecalis* was inoculated on the plates, the CFU count decreased with increasing concentrations of Esomeprazole. The CFU on agar plates are significantly more than 300 colonies, the short form of too numerous to count (TNTC) may be entered in the results. A total of 52 colonies were grown in 10 µg/mL of Esomeprazole in LB

plates (**Figure S4**) no colonies were observed in 20 μg/mL plates. Previously *Luigi Gatta (2003)* reported Esomeprazole is an enantiomorph of Esomeprazole, which is a benzaldehyde derivative inhibits gastric acid secretion, through this inhibitory activity, it inactivates the intestinal Gram negative bacteria *Helicobacter pylori* [59 -60]. Among the computationally screened drugs, Amoxicillin is a β- lactam ring containing antibiotic used for bacterial infections, prevention and the treatment of anthrax. It also showed the antibacterial activity against the Penicillin resistant strains such as Gram positive *S. pneumoniae* and Gram negative bacteria *Pneumococci*, *Haemophilus influenzae* and *Moraxella catarrhalis*, When Amoxicillin was combined with the clavulanate, amoxicillin/clavulanate product to which the greatest percentage of susceptibility and resistant strains of *Pneumococci* [61]. In addition the Amoxicillin/Clavulanate combination derived product has the good antibacterial activity against the Gram positive bacteria *E. faecalis* [62]. This Amoxicillin/Clavulanate activity was compared with the already reported antimicrobial agents [63]. Ciprofloxacin and Cefaxime showed the excellent activity against methicillin-susceptible *S. aureus*, methicillin-sensitive *S. epidermidis*. These four compounds inhibition rate was indicated through growth curve is shown in figure 7, which clearly shows that the involvement of these screened compounds against the *E. faecalis*

Effect of screened drugs on biofilm formation

Based on the BIC of the screened drugs the effective concentration (30-40 μg/ml) was determined using microscopy. The results of light microscopic analysis revealed that the control slides showed a well-developed biofilm growth of test bacterial pathogens whereas bacterial pathogens treated with the screened drugs showed the reduced biofilm on glass surface and inhibit the bacterial cells growth at the BIC concentration (40 μg/ml). Bacterial biofilm was

inhibited by screened drugs; among these Esomeprazole showed the potential activity and showed the poor biofilm growth (90 %) when compared to the other screened drugs and control sample (**Figure 7**). Followed by the Esomeprazole, Amoxillin showed the effective biofilm inhibition (80 %), Cephalexin and Cefixime exhibited the same inhibitory activity towards the pathogen (40-50 % of biofilm reduction). Further, the CLSM analysis showed loose biofilm architecture of bacterial pathogens when treated with Esomeprazole, Amoxicillin, Cephalexin and Cefaxime at the concentration of 40 μg/ml and control (**Figure 8**). The control biofilms showed a higher surface coverage as bacterial surface was disrupted by the screened drugs and arrests the bacterial cells growth on the surface of the glass slides. Light microscopy results were confirmed with the topography and surface morphology images of Confocal Laser Scanning Microscopy (CLSM). Similarly the both light and CLSM results of antibiofilm activity of Esomeprazole against Gram positive *E. faecalis* was cross checked through scanning electron microscopy (SEM). The SEM surface morphology indicated that dense and aggregated biofilm occur in the control slides which could be due to the production of exopolyscachharide in *E. faecalis.* When visualized under the microscopy it looks carpet (sheet) like structure and the bacterial cells were embedded in the EPS carpet layer on the surface of the glass pieces in the control *E. faecalis* (**Figure 9**). The best compounds on biofilm inhibitions were checked for its percent inhibition of biofilm against the screened compounds concentration and results are interpreted in **Figure 10a and 10b**. Even though Amoxicillin is already reported as antibiotic compounds, one of our screened compounds and Esomeprazole shows much better inhibition.

Esomeprazole showed the good anti biofilm inhibition against the Gram positive pathogen *E. faecalis*. When compared with Amoxicillin, Esomeprazole shows 80% extra inhibition towards the *E. faecalis* biofilm and this is clearly shown in the Figure 8a and 8b. Esomeprazole is

osmeprazole family benzaldehyde drug interacts with the bacterial cells and inhibit the growth of the bacteria concurrently. Our results were synchronized with the already reported Vandana Singh et al. 2012 investigation. In this, nosocomial infections causing pathogens such as *S. aureus* and *P. aeruginosa* and its biofilm was inhibited Proton pump inhibitor Esomeprazole [64].

In early studies Nguyen et al., who investigated the use of benzimidazole PPI against biofilm-embedded *S. mutans* [65]. Commonly the benzaldehyde and benzaldehyde based derivatives have the anti biofilm activity. Recently, Sambanthamoorthy et al. (2011) have identified a novel benzimidazole that inhibits bacterial biofilm formation [66]. β-lactam antibiotic *Amoxicillin* had the good antibacterial activity, but it could not able to invade the bacterial biofilm cells alone, when combined with the other antibiotic drugs such as Ibuprofen, N-acetyl-L-cysteine, *Amoxicillin*, Erythromycin, and levofloxacin it showed the anti biofilm activity against *S. pneumoniae* strains [67]. Similarly, *Ciprofloxacin* also synergistically combined with the Triclosan, reduces the *Salmonella typhimurium* biofilm, in this triclosan weakens the bacterial cells; ciprophalaxin induces the bacterial cell wall permeability [68]. From these compounds we have finally noticed that Esomeprazole and Ampicillin are having potential anti biofilm activity against the *E. faecalis.*

Conclusion

Current study explained the unavailability of solved SrtA structures in *E. faecalis* which plays the core role in the biofilm formations and cell wall incorporation mechanisms. In this work, we exploited the homology modeling techniques for predicting the structure of SrtA and additionally screened the potential compounds against its microbial and biofilm activity. A large scale 100ns molecular dynamics simulations suggest the stable conformations and stable conformation based screening provides best compounds through scoring methods. The interactions were validated

with multiple conformations of flexible proteins, which finally show that screened compounds have potential bonding interactions. From our screening, we understand that all the compounds have great potency of scoring, energy and interaction parameters. Dynamic interaction behavior of best compounds provides the strong bonding interaction occurs between the protein and ligand throughout the timescale. Such study provides an important estimation of intra-molecular properties of inhibitor that can trigger the biological response. Some of the screened compounds like ampicillin are well known antibiotics are passed through our screening suggest that our screening is properly validated. Validation of screening was executed using anti-microbial and anti-biofilm activity studies. When comparing with known antibiotic amoxicillin, the esomeprazole was found to have better potential towards microbial activity and biofilm formation. Additionally, Cefixime and Cephalexin also has inhibitory activity against the microbes and biofilm formation. Further atom level modification in these inhibitors will definitely provide enhanced SrtA inhibitors against *E. faecalis*. By this approach, we conclude that obtained homology model seems to be perfect for the experimental studies and additionally, we report few potent compounds which significantly inhibit the activity of microbial and biofilm formation in *E. faecalis*. These new insights promotes the SrtA as “Universal Drug Target” by the inhibition of pathogenic bacteria’s with highest success rate for designing the potent inhibitors against this target.

Conflict of Interests: None

Acknowledgements: The authors thankfully acknowledge the CSIR for research funding and fellowship grants (Ref. No: 37(1491)/11/EMR-II). One of the authors Chandrabose Selvaraj gratefully acknowledges CSIR for the Senior Research Fellowship (SRF). The authors thankfully acknowledge the Dr. Prashanth Suravajhala (Bioclues Organization, IKP Knowledge Park, Hyderabad, 500009 Andhra Pradesh, India) and Ms. Bharathi Priya, M. Phil Scholar, Dept of Bioinformatics, Alagappa University for their wonderful help in manuscript preparation.

Reference

1. A. Ronald, *Am J Med* **2002,** 113 Suppl 1A, 14S-19S.
2. A. Ronald, *Dis Mon* **2003,** 49, (2), 71-82.
3. T. D. Allen, D. R. Moore, X. Wang, V. Casu, R. May, M. R. Lerner, C. Houchen, D. J. Brackett, M. M. Huycke, *J Med Microbiol* **2008,** 57, (Pt 10), 1193-204.
4. S. A. Chowdhury, C. A. Arias, S. R. Nallapareddy, J. Reyes, R. J. Willems, B. E. Murray, *J Clin Microbiol* **2009,** 47, (9), 2713-9
5. R. C. Matos, N. Lapaque, L. Rigottier-Gois, L. Debarbieux, T. Meylheuc, B. Gonzalez-Zorn, F. Repoila, F. Lopes Mde, P. Serror, PLoS Genet **2013,** 9, (6), e1003539.
6. A. Singh, R. V. Goering, S. Simjee, S. L. Foley, M. J. Zervos, *Clin Microbiol Rev* **2006,** 19, (3), 512-30.
7. A. L. Kau, S. M. Martin, W. Lyon, E. Hayes, M. G. Caparon, S. J. Hultgren, *Infect Immun* **2005,** 73, (4), 2461-8.
8. N. Tsuchimori, T. Yamazaki, K. Okonogi, *J Antimicrob Chemother* **1997,** 39, (3), 423-5.
9. L. A. Bohle, T. Riaz, W. Egge-Jacobsen, M. Skaugen, O. L. Busk, V. G. Eijsink, G. Mathiesen, *BMC Genomics* **2013,** 12, 135.
10. E. K. Call, T. R. Klaenhammer, *Front Microbiol* **2013,** 4, 73.
11. P. S. Guiton, T. J. Hannan, B. Ford, M. G. Caparon, S. J. Hultgren, *Infect Immun* **2013.** 81, (1), 329-39.
12. P. S. Guiton, C. S. Hung, L. E. Hancock, M. G. Caparon, S. J. Hultgren, *Infect Immun* **2010,** 78, (10), 4166-75.
13. P. S. Guiton, C. S. Hung, K. A. Kline, R. Roth, A. L. Kau, E. Hayes, J. Heuser, K. W. Dodson, M. G. Caparon, S. J. Hultgren, *Infect Immun* **2009,** 77, (9), 3626-38.

14. H. J. Kang, F. Coulibaly, T. Proft, E. N. Baker, *PLoS One* **2011,** 6, (1), e15969.

15. C. M. Levesque, E. Voronejskaia, Y. C. Huang, R. W. Mair, R. P. Ellen, D. G. Cvitkovitch, *Infect Immun* **2005,** 73, (6), 3773-7.

16. E. Tsompanidou, E. L. Denham, M. J. Sibbald, X. M. Yang, J. Seinen, A. W. Friedrich, G. Buist, J. M. van Dijl, PLoS One **2012,** 7, (9), e44646.

17. Y. Konto-Ghiorghi, E. Mairey, A. Mallet, G. Dumenil, E. Caliot, P. Trieu-Cuot, S. Dramsi, *PLoS Pathog* **2009,** 5, (5), e1000422.

18. A. H. Nobbs, R. M. Vajna, J. R. Johnson, Y. Zhang, S. L. Erlandsen, M. W. Oli, J. Kreth, L. J. Brady, M. C. Herzberg, *Microbiology* **2007,** 153, (Pt 12), 4088-97.

19. L. A. Marraffini, A. C. Dedent, O. Schneewind, *Microbiol Mol Biol Rev* **2006,** 70, (1), 192-221.

20. A. Kishen, M. Upadya, G. P. Tegos, M. R. Hamblin, *Photochem Photobiol* **2010,** 86, (6), 1343-9.

21. J. A. Mohamed, D. B. Huang, *J Med Microbiol* **2007,** 56, (Pt 12), 1581-8.

22. A. A. Ramadhan, E. Hegedus, *J Clin Pathol* **2005,** 58, (7), 685-6.

23. R. R. Dai, Y. Yang, L. Y. Xiong, J. J. Li, T. P. Quan, Q. Yu, *Sichuan Da Xue Xue Bao Yi Xue Ban* **2010,** 41, (5), 827-30.

24. P. S. Guiton, C. S. Hung, K. A. Kline, R. Roth, A. L. Kau, E. Hayes, J. Heuser, K. W. Dodson, M. G. Caparon, S. J. Hultgren, *Infect Immun* **2009,** 77, (9), 3626-38.

25. C. J. Kristich, D. A. Manias, G. M. Dunny, *Appl Environ Microbiol* **2005,** 71, (10), 5837-49.

26. C. Selvaraj, S. K. Singh, J Biomol Struct Dyn. **2013,** doi:10.1080/07391102.2013.818577.

27. S. Pronk, S. Pall, R. Schulz, P. Larsson, P. Bjelkmar, R. Apostolov, M. R. Shirts, J. C. Smith, P. M. Kasson, D. van der Spoel, B. Hess, E. Lindahl, *Bioinformatics* **2013,** 29, (7), 845-54.

28. Maestro, version 9.3, Schrödinger, LLC, New York, NY, 2012.

29. D. W. Mount. *CSH Protoc* **2007,** pdb top17.

30. N. Fernandez-Fuentes, B. K. Rai, C. J. Madrid-Aliste, J. E. Fajardo, A. Fiser, *Bioinformatics* **2007,** 23, (19), 2558-65.

31. D. Frishman, P. Argos, *Proteins* **1995,** 23, (4), 566-79.

32. P. Gouet, X. Robert, E. Courcelle, *Nucleic Acids Res* **2003,** 31, (13), 3320-3.

33. N. Eswar, B. Webb, M. A. Marti-Renom, M. S. Madhusudhan, D. Eramian, M. Y. Shen, U. Pieper, A. Sali, *Curr Protoc Protein Sci* **2007,** Chapter 2, Unit 2 9.

34. B. R. Sahoo, B. Swain, M. Basu, P. Panda, N. K. Maiti, M. Samanta, J Mol Model **2012,** 18, (5), 1713-22.

35. E. F. Pettersen, T. D. Goddard, C. C. Huang, G. S. Couch, D. M. Greenblatt, E. C. Meng, T. E. Ferrin, *J Comput Chem* **2004,** 25, (13), 1605-12.

36. D. J. Huggins, *J Chem Phys* **2012,** 136, (6), 064518.

37. R. M. Shafreen, C. Selvaraj, S. K. Singh, S. K. Pandian, *J Mol Recognit* **2013,** 26, (6), 276-85.

38. A. W. Schuttelkopf, D. M. van Aalten, *Acta Crystallogr D Biol Crystallogr* **2004,** 60, (Pt 8), 1355-63.

39. S. C. Flores, M. B. Gerstein, *BMC Bioinformatics* **2012,** 12, 417.

40. M. R. Housaindokht, M. R. Bozorgmehr, M. Bahrololoom, *J Theor Biol* **2008,** 254, (2), 294-300.

41. C. Selvaraj, S.K. Singh, S.K. Tripathi, K.K. Reddy, M. Rama. *Med Chem Res* **2012,** 21 (12): 4060-4068.

42. T. A. Halgren, *J Chem Inf Model* **2009,** 49, (2), 377-89.

43. P. Vijayalakshmi, C. Selvaraj, S. K. Singh, J. Nisha, K. Saipriya, P. Daisy, *J Biomol Struct Dyn* **2013,** 31, (6), 561-71.

44. S. Kawatkar, H. Wang, R. Czerminski, D. Joseph-McCarthy, *J Comput Aided Mol Des* **2009,** 23, (8), 527-39.

45. D. S. Wishart, C. Knox, A. C. Guo, S. Shrivastava, M. Hassanali, P. Stothard, Z. Chang, J. Woolsey, *Nucleic Acids Res* **2006,** 34, (Database issue), D668-72.

46. S.K. Tripathi, C. Selvaraj, S.K. Singh, K.K. Reddy. *Med Chem Res* **2012,** 21 (12): 4239-4251.

47. R. A. Friesner, R. B. Murphy, M. P. Repasky, L. L. Frye, J. R. Greenwood, T. A. Halgren, P. C. Sanschagrin, D. T. Mainz, *J Med Chem* **2006,** 49, (21), 6177-96.

48. M. Totrov, R. Abagyan, *Curr Opin Struct Biol* **2008,** 18, (2), 178-84.

49. A. M. Ferrari, B. Q. Wei, L. Costantino, B. K. Shoichet, *J Med Chem* **2004,** 47, (21), 5076-84.

50. M. Y. Mizutani, Y. Takamatsu, T. Ichinose, K. Nakamura, A. Itai, *Proteins* **2006,** 63, (4), 878-91.

51. C. N. Cavasotto, R. A. Abagyan, *J Mol Biol* **2004,** 337, (1), 209-25.

52. W. Sherman, T. Day, M. P. Jacobson, R. A. Friesner, R. Farid, *J Med Chem* **2006,** 49, (2), 534-53.

53. D. L. Mobley, K. A. Dill, *Structure* **2009,** 17, (4), 489-98.

54. J. Jakubik, A. Randakova, V. Dolezal, *J Comput Aided Mol Des* **2013,** 27, (6), 525-38.

55. D. Das, Y. Koh, Y. Tojo, A. K. Ghosh, H. Mitsuya, *J Chem Inf Model* **2009,** 49, (12), 2851-62.

56. S. K. Tripathi, S. K. Singh, P. Singh, P. Chellaperumal, K. K. Reddy, C. Selvaraj, *J Mol Recognit* 25, (10), 504-12.

57. L. Baldassarri, R. Creti, S. Recchia, M. Imperi, B. Facinelli, E. Giovanetti, M. Pataracchia, G. Alfarone, G. Orefici, *J Clin Microbiol* **2006,** 44, (8), 2721-7.

58. R. A. Friesner, J. L. Banks, R. B. Murphy, T. A. Halgren, J. J. Klicic, D. T. Mainz, & P. S. Shenkin, *Jour of med chem* **2004,** 47, (7), 1739-1749.

59. L. Gatta, F. Perna, N. Figura, C. Ricci, J. Holton, L. D'Anna, M. Miglioli, D. Vaira, *J Antimicrob Chemother* **2003,** 51, (2), 439-42.

60. G. K. Anagnostopoulos, S. Tsiakos, G. Margantinis, P. Kostopoulos, D. Arvanitidis, *J Clin Gastroenterol* **2004,** 38, (6), 503-6.

61. M. Peric, F. A. Browne, M. R. Jacobs, P. C. Appelbaum, *Clin Ther* **2003,** 25, (1), 169-77.

62. M. Bassetti, L. M. Dembry, P. A. Farrel, D. A. Callan, V. T. Andriole, *Diagn Microbiol Infect Dis* **2001,** 41, (3), 143-8.

63. M. N. Zubkov, V. E. Nonikov, E. N. Gugutsidze, T. M. Sutormina, O. V. Makarova, *Antibiot Khimioter* **1992,** 37, (9), 34-6.

64. V. Singh, V. Arora, M. J. Alam, K. W. Garey, *Antimicrob Agents Chemother* **2012,** 56, (8), 4360-4.

65. P. T. Nguyen, J. D. Baldeck, J. Olsson, R. E. Marquis, *Oral Microbiol Immunol* **2005,** 20, (2), 93-100.

66. K. Sambanthamoorthy, A. A. Gokhale, W. Lao, V. Parashar, M. B. Neiditch, M. F. Semmelhack, I. Lee, C. M. Waters, *Antimicrob Agents Chemother* **2011,** 55, (9), 4369-78.

67. G. del Prado, V. Ruiz, P. Naves, V. Rodriguez-Cerrato, F. Soriano, M. del Carmen Ponte, *Diagn Microbiol Infect Dis* **2010,** 67, (4), 311-8.

68. M. Tabak, K. Scher, M. L. Chikindas, S. Yaron, *FEMS Microbiol Lett* **2009,** 301, (1), 69-76.

Table legends

Table 1. Scoring values and interactions of screened compounds against the SrtA

Table 2. Atomic view of interactions between screened compounds against SrtA

Table 3. Anti microbial activity for screened compounds against *Enterococcus faecalis*

Table 1

Ligand Name	Docking Score (Kcal/mol)	Docking Energy (Kcal/mol)	IFD score	Binding Energy (Kcal/ mol)	H-bonds	Non Bonded Interactions	Hydrophobic bonds	Interacting Residues
Amoxicillin	-10.10	-57.45	-331.11	-63.48	6	13	249	LEU2, ASP46, CYS136, ARG145
Cefixime	-10.53	-84.01	-330.95	-73.34	10	10	270	SER1, GLU4, GLY5, CYS136, THR135, LYS141, ARG145
Esomeprazole	-8.95	-51.87	-330.06	-68.45	3	8	254	MET117, ARG145
Cephalaxin	-8.89	-62.27	-328.72	-59.57	5	4	248	SER1, LEU2, CYS136, LYS141, ARG145
Losartran	-7.52	-48.38	-327.54	-43.57	3	9	268	GLY5, ASP46, ARG145

Table 2

Ligand Name	Interactions	Distance (Å)
Amoxicillin	LEU2(O)O---(H)	1.867
	LEU2(O)O---(H)	2.096
	ASP46 (O)O---(H)	1.913
	CYS136(H)H---(O)	1.632
	ARG145(H)H---(O)	2.116
	ARG145(H)H---(O)	1.886
Cefixime	SER1(H)H---(O)	2.122
	SER1(H)H---(O)	2.481
	SER1(H)H---(O)	2.189
	GLU4(O)O---(H)	1.909
	GLY5(O)O---(H)	2.474
	CYS136(O)O---(H)	2.224
	THR135(O)---(H)	1.999
	LYS141(H)---(N)	2.285
	LYS141(H)---(N)	2.333
	ARG145(H)---(O)	1.603
Esomeprazole	MET117(O)O---(H)	1.972
	ARG145(H)H---(O)	2.214
	ARG145(H)H---(O)	1.996
Cephalaxin	SER1(H)H---(S)	2.254
	LEU2(O)O---(H)	1.727
	CYS136(O)O---(H)	1.849

Table 3

Microorganisms	**Samples**	**Zone of inhibition (mm in diameter)**	**Disc diffusion (mm in diameter)**
	Esomeprazole	17.3±0.53	16±0.5
	Amoxicillin	16±0.46	15.4±0.5
	Cephalaxin	15.8±0.26	15±0.1
	Cefixime	14.8±0.7	12±0.5
	Amlodipine	14±0.2	11.2±0.5
Enterococcus	Enalapril	13±0.5	11±0.4
faecalis	Ampicillin	11.5±0.12	10±0.5
	Gilipizide	11±0.4	10.5±0.1
	Chloramphenical	10.5±0.2	10.5±0.7
	Losartran	10±0.7	9±0.7

Legend for Figures

Figure 1: **(I)** SrtA intended for cell wall anchoring are first initiated into the Sec pathway by an N-terminal signal peptide (LPXTG: X indicates potential points of inhibition in the "sorting pathway"). **(II & III)** Thioester-linked acyl-enzyme intermediate is formed between sortase and C-terminal threonine of surface protein. **(IV)** Acyl-enzyme occurs through nucleophilic attack of the amino group of the pentaglycine of lipid II to generate lipid II-linked surface protein. **(V)** Cell wall incorporation through progress of SrtA transpeptidation. The black tail represents the hydrophobic domain, followed by positively charged tail of cell wall sorting signals.

Figure 2: Sequence alignment of SrtA with its template sequences and secondary structure alignment predicted through ClustalW and Espript

Figure 3a: Homology modeled structure of SrtA from *E. faecalis* view through PyMol secondary structure visualization.

3b: Target (Red) and Template (Green) matching through Chimera.

Figure 4a: RMSD graph of modeled SrtA structure for 100ns of timescale with Zoomed view of deviations from 40-100ns

4b: RMSF plot showing residue vise fluctuations of modeled SrtA with respect to 100ns of timescale

4c : Hydrogen bond interaction between modeled protein and water model (A) Hydrogen bonds pairs of with system water molecules within 0.35nm and >0.35nm. (B) The graph indicates the average values obtained during the entire period of simulation for modeled protein hydrogen bond pairing with system

Figure 5: Represents the IFD docking interactions of screened compounds against SrtA (A) Amoxicillin, (B) Cephalaxin, (C) Cefixime, and (D) Esomeprazole

Figure 6a: RMSD graph of screened compounds against the SrtA with respect to timescale of 20ns

6b: Ligand RMSD graph of screened compounds with respect to timescale of 20ns

6c: RMSF plot of SrtA with screened compounds

6d: RMSF plot of ligand atoms showing conformational changes

6e: Hydrogen bond interactions between SrtA and screened compounds with respect to timescale of 20ns

Figure 7: Growth curve of microbes inhibited with our screened compounds (A) amoxicillin, (B) cephalaxin, (C) cefixime, and (D) esomeprazole

Figure 8: Light and CLSM visualization of *E. faecalis* biofilm inhibition using the screened drugs (A) Amoxicillin, (B) Cephalaxin, (C) Cefixime, and (D) Esomeprazole

Figure 9: Surface morphology of *E. faecalis* biofilm showed the control and esomeprazole treated biofilm in SEM

Figure 10: Percentage of *E. faecalis* Biofilm inhibition using a (A) amoxicillin and (B) esomeprazole

Figure 1

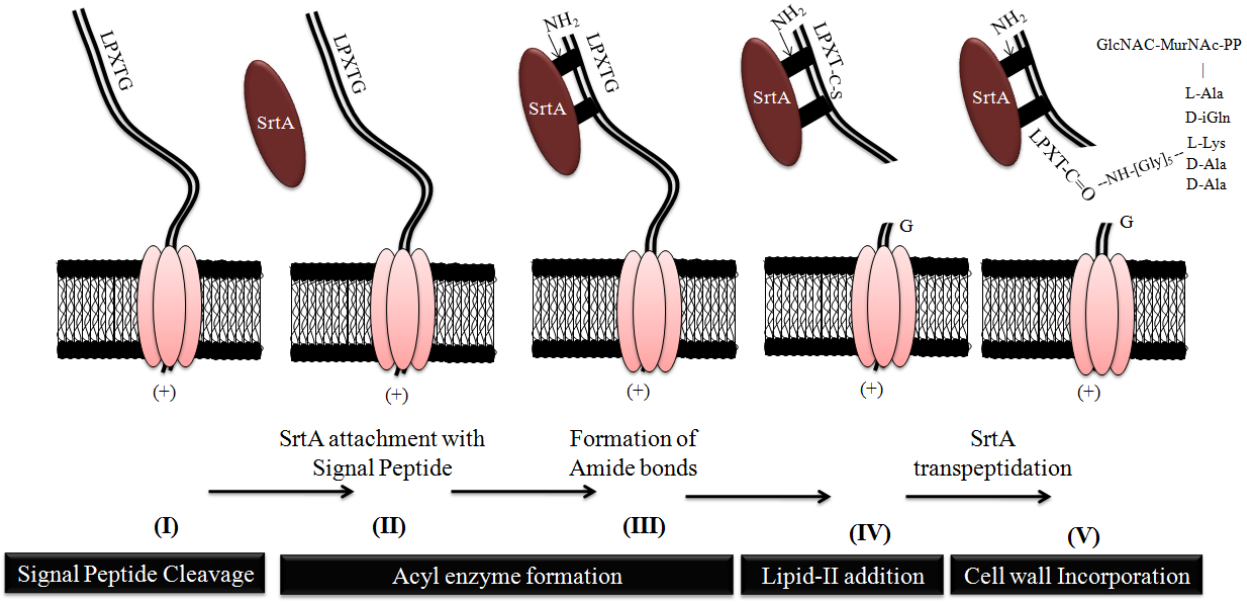

Figure 2

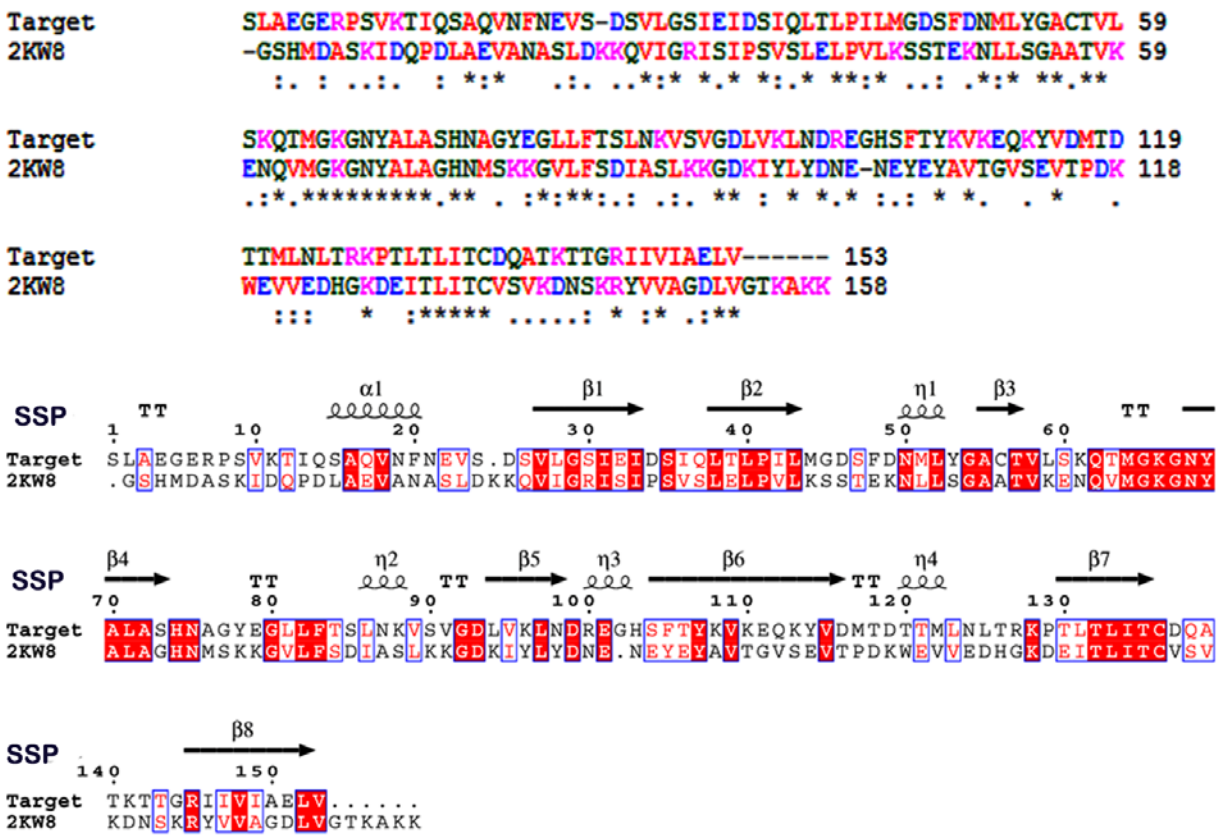

Figure 3

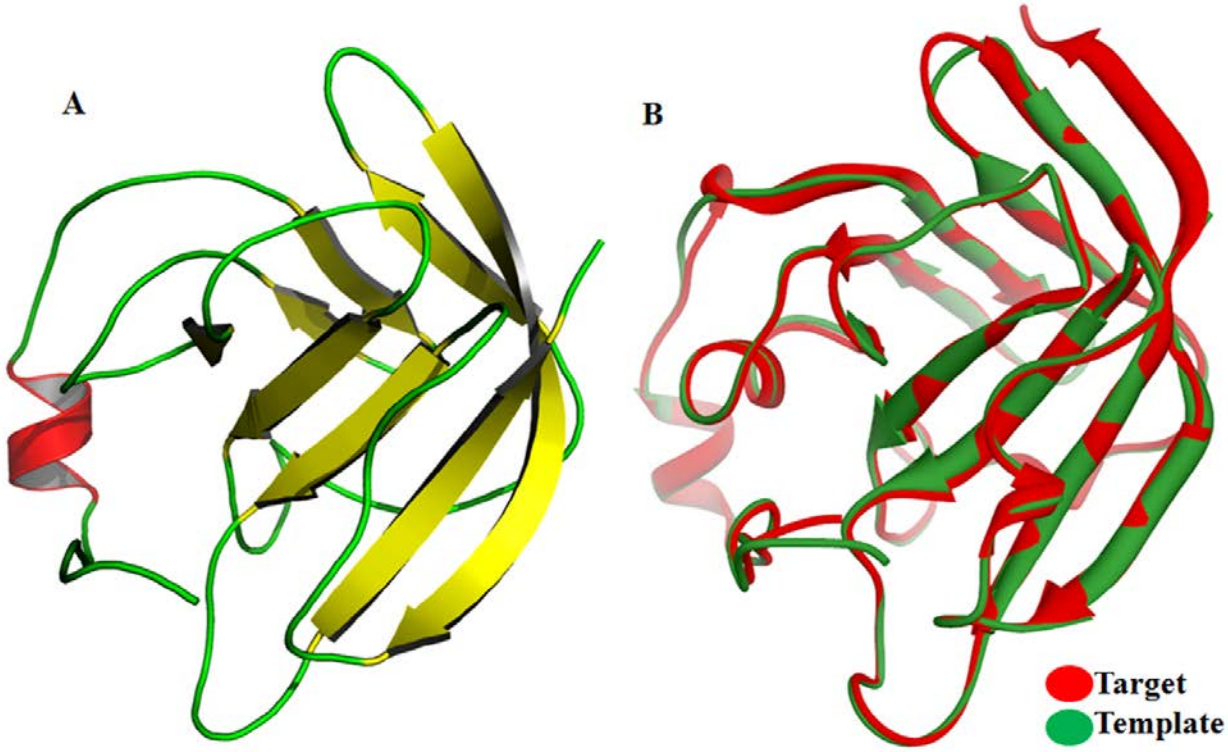

Figure 4a

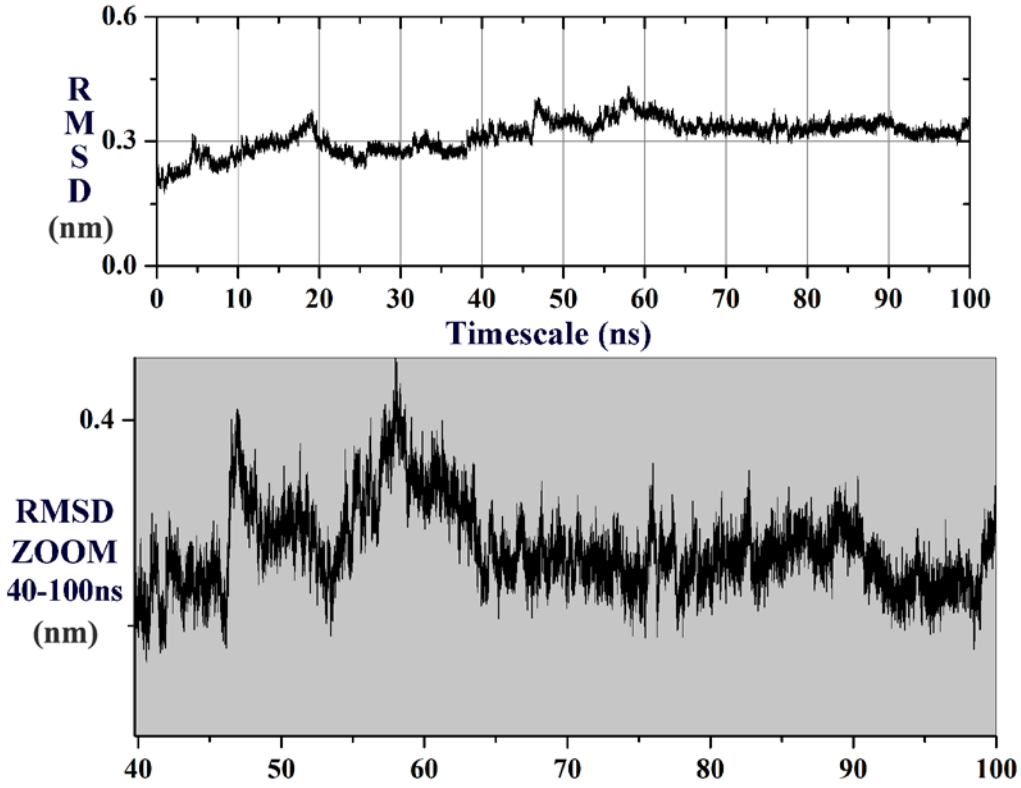

Figure 4b

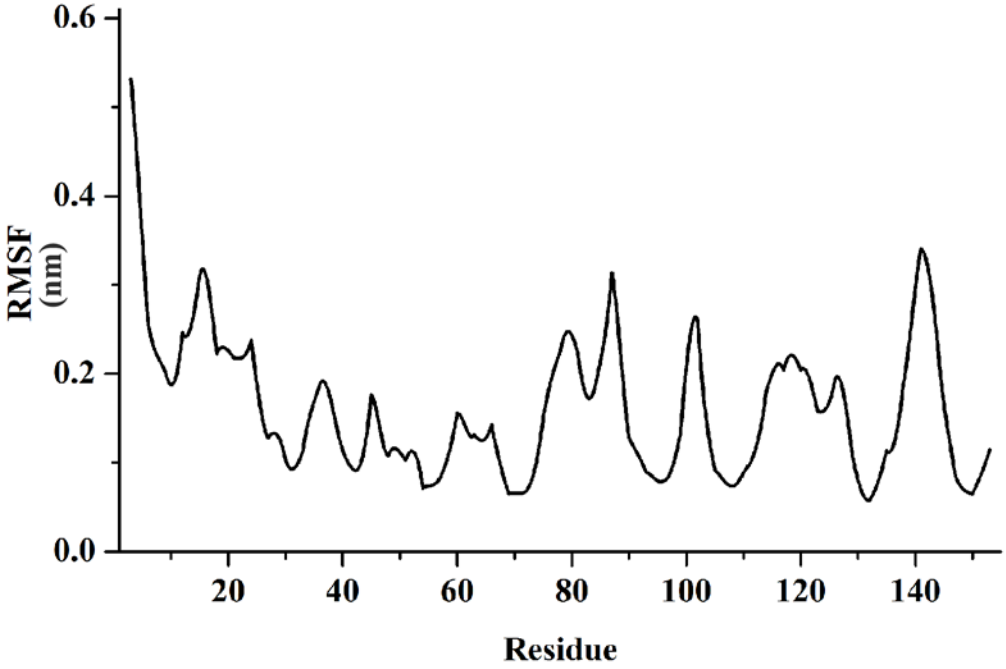

Figure 4C

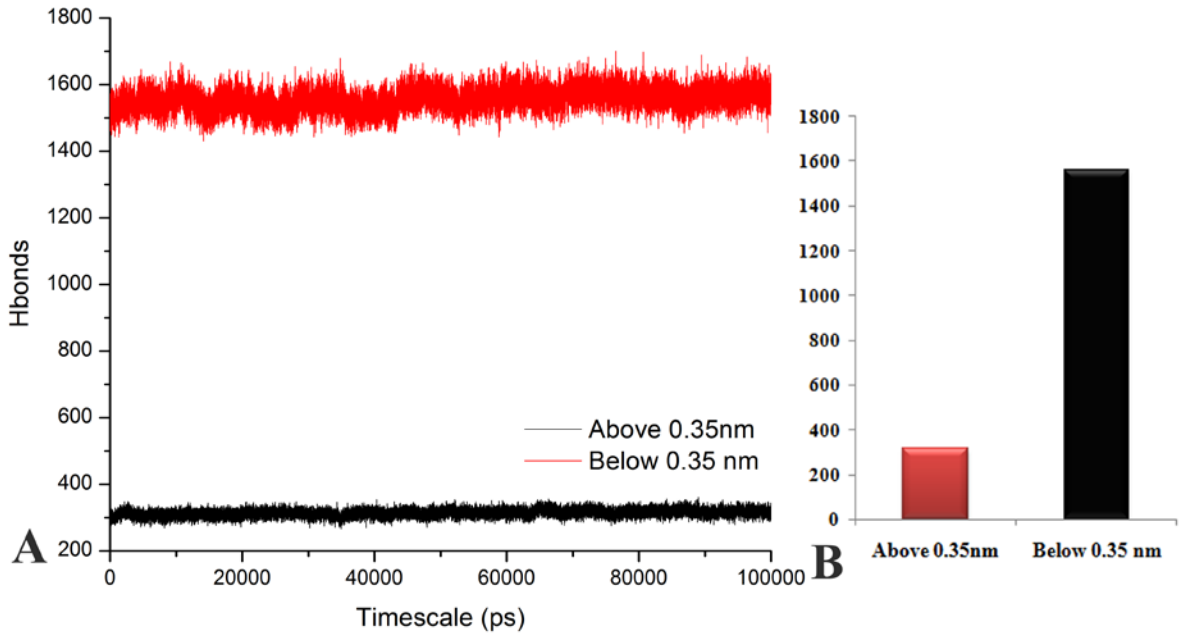

Figure 5

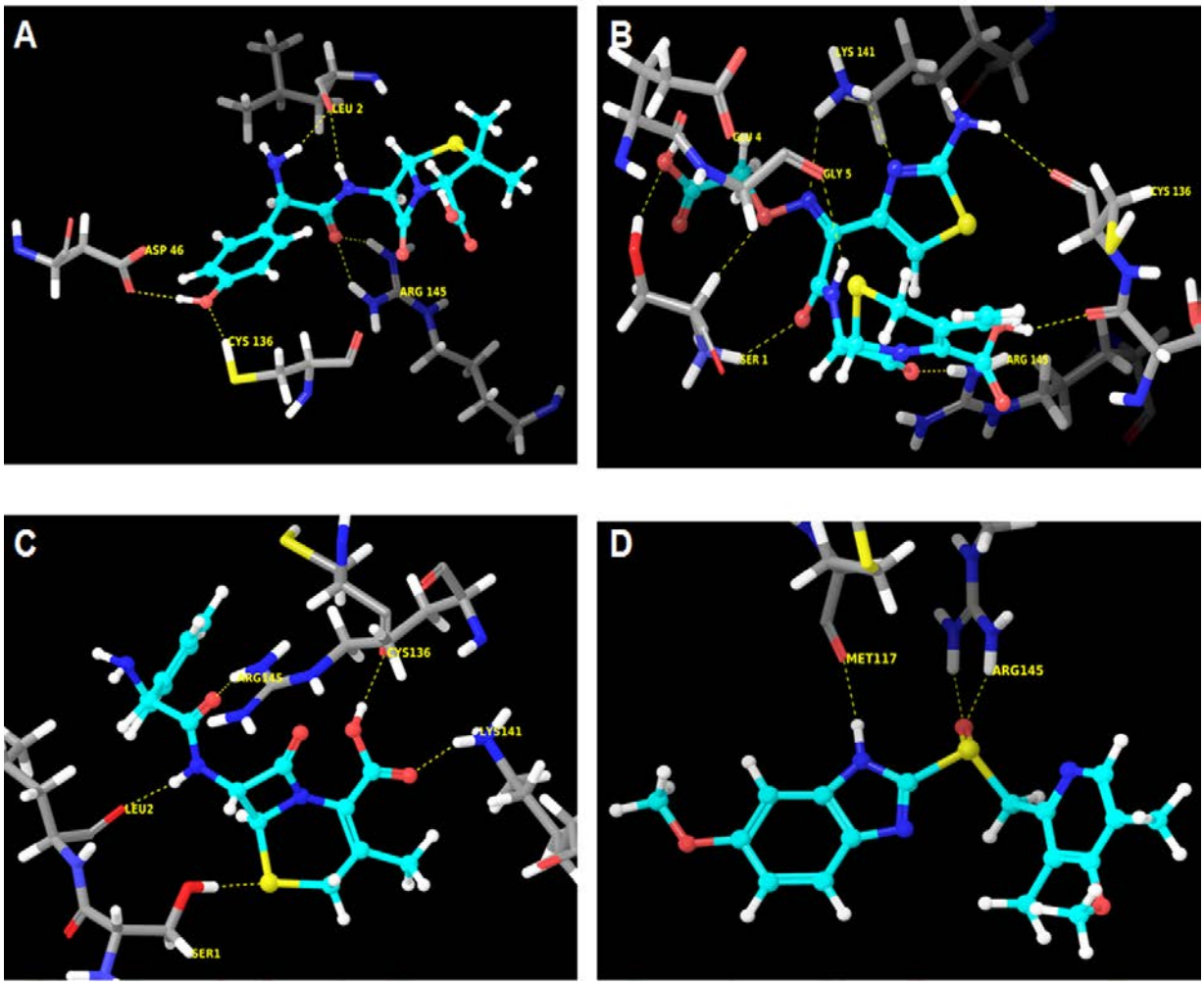

Figure 6a

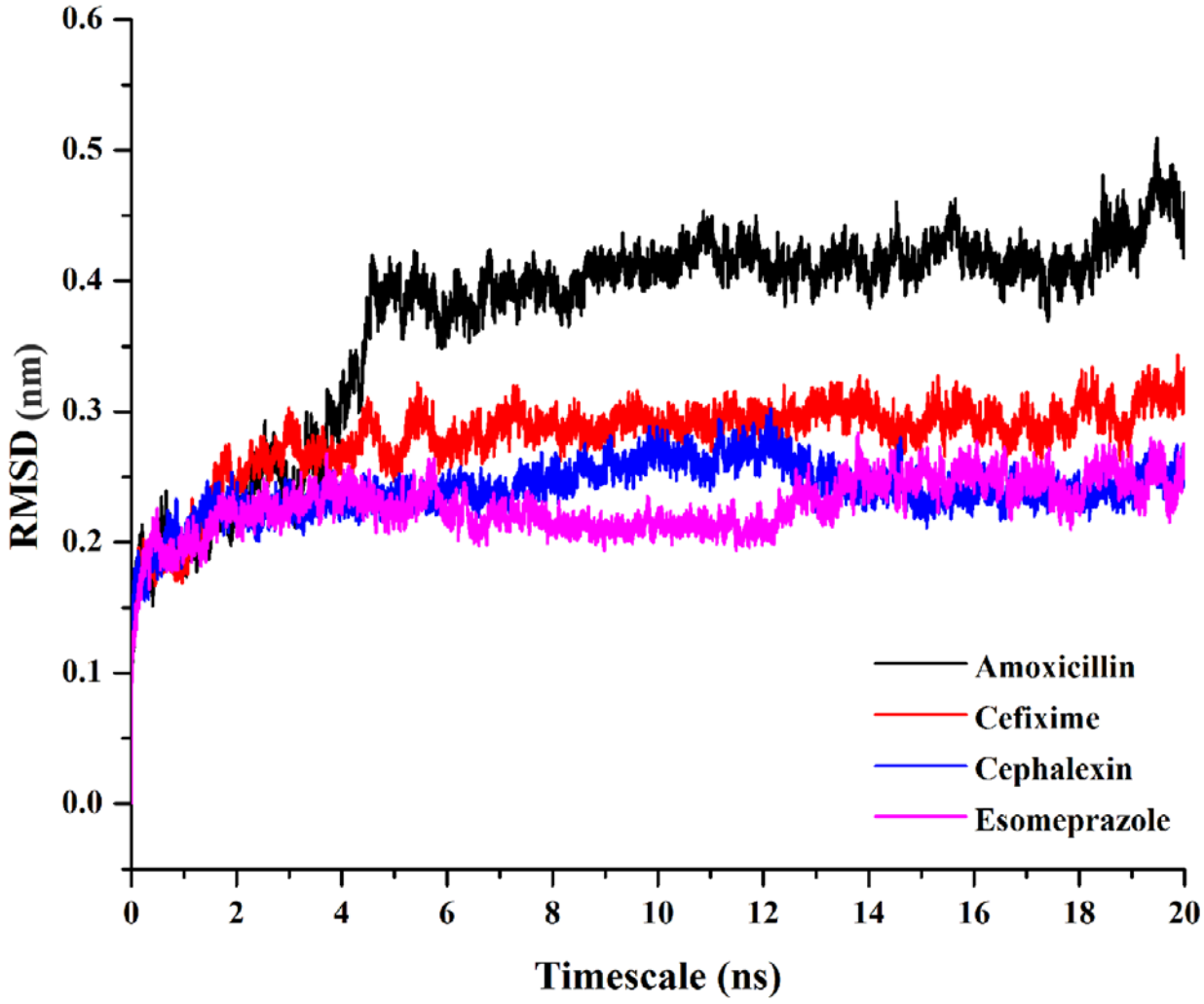

Figure 6b

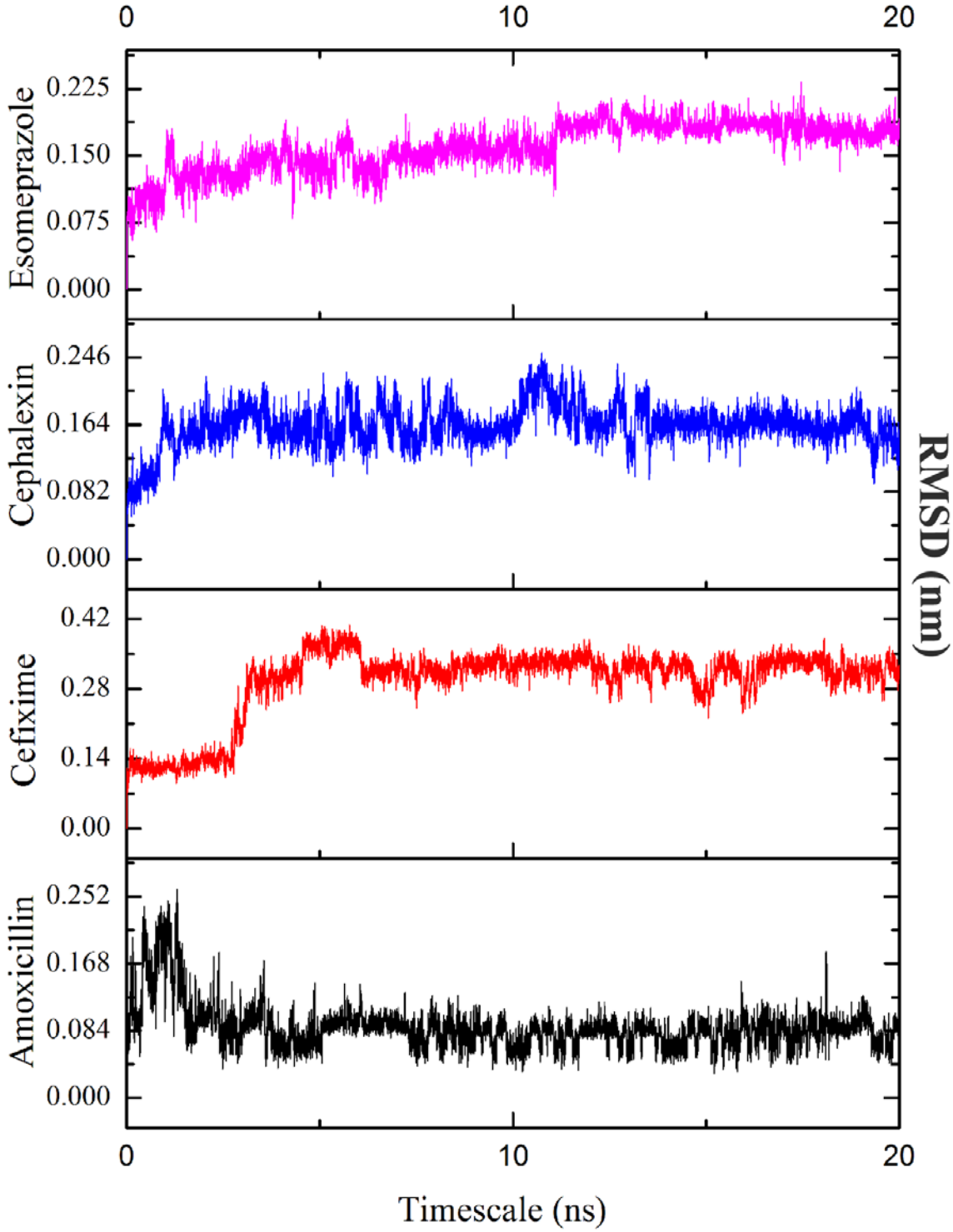

Figure 6c

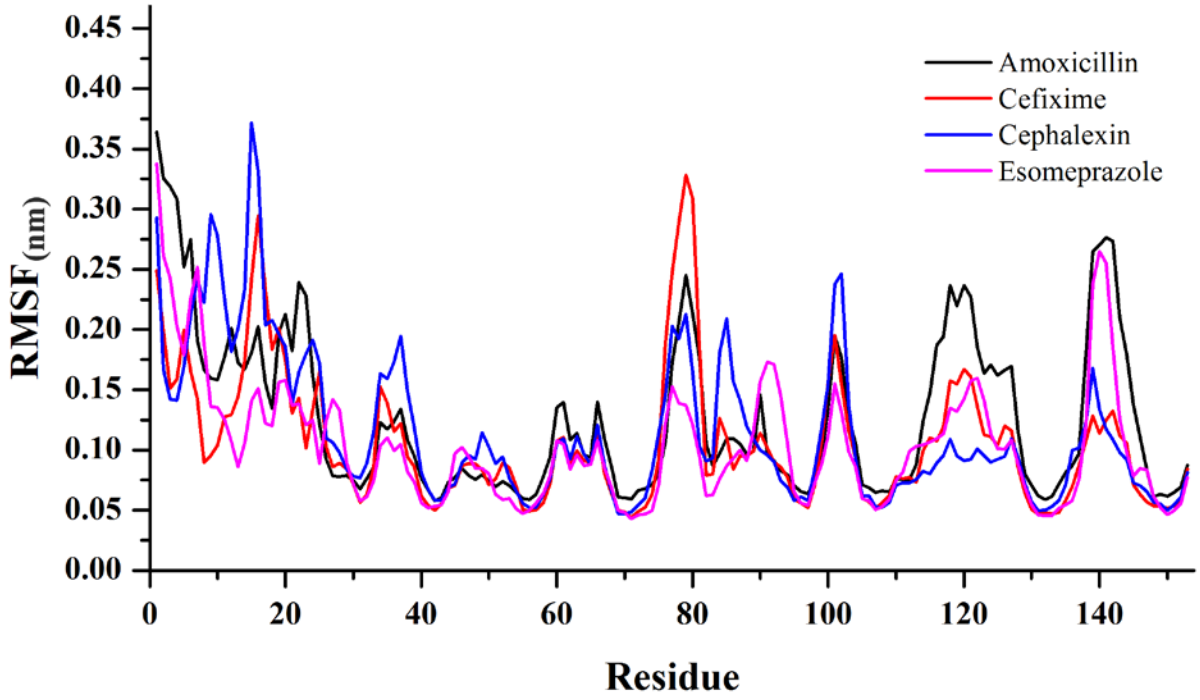

Figure 6d

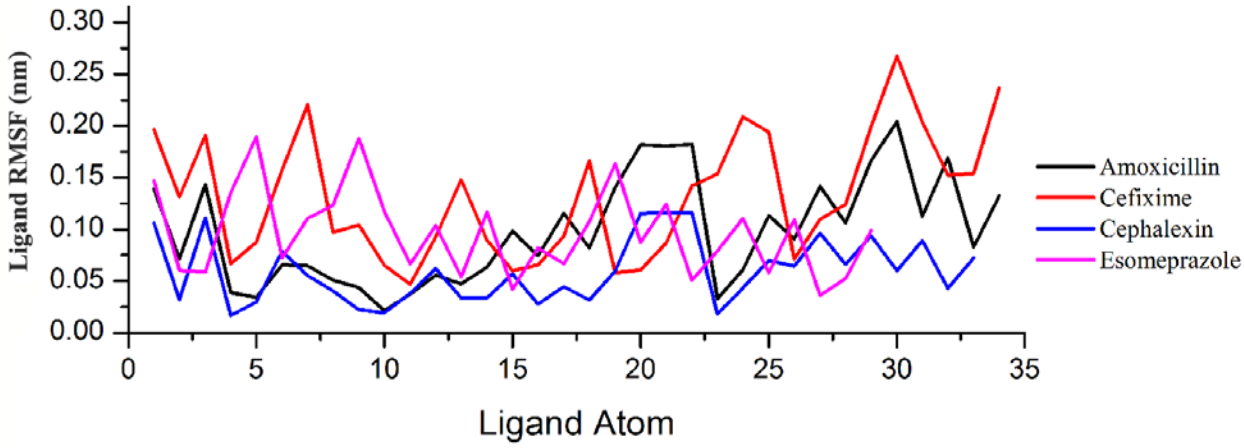

Figure 6e

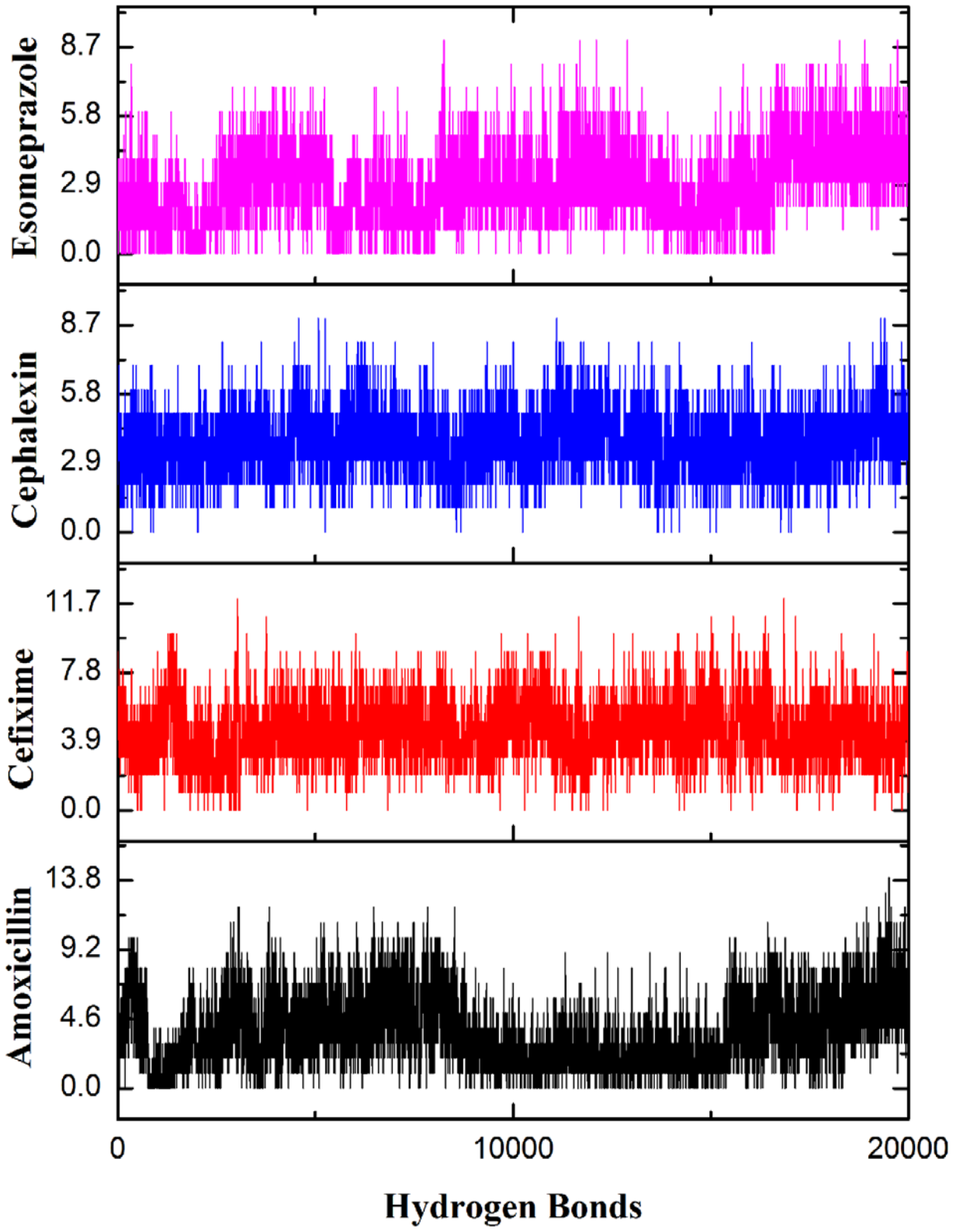

Figure 7

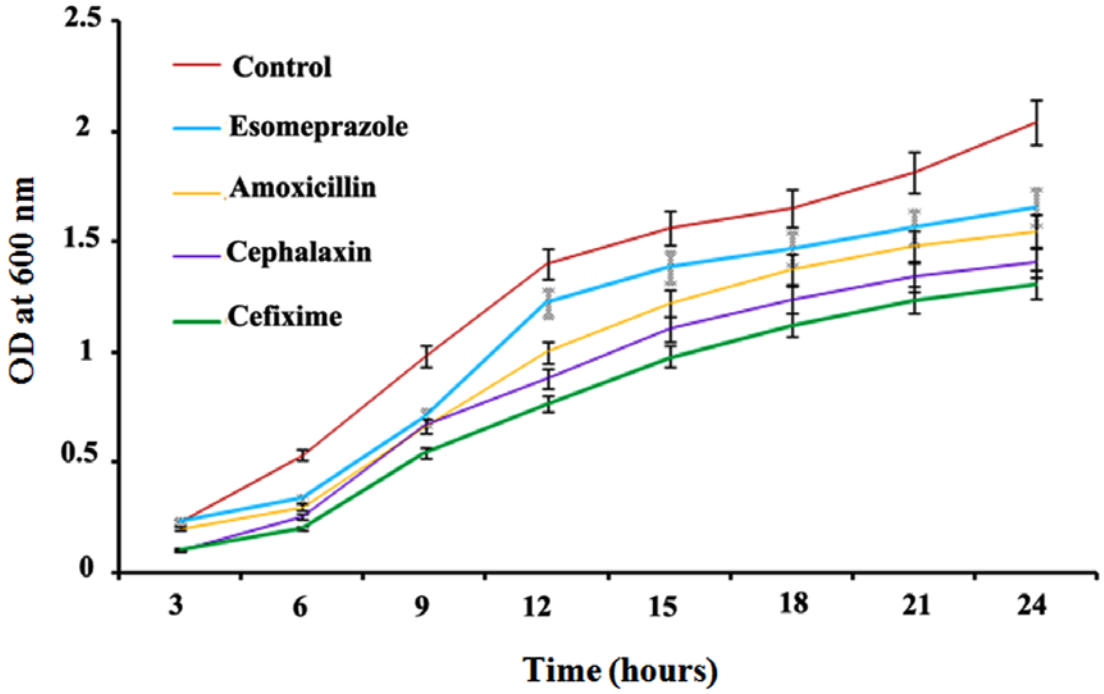

Figure 8

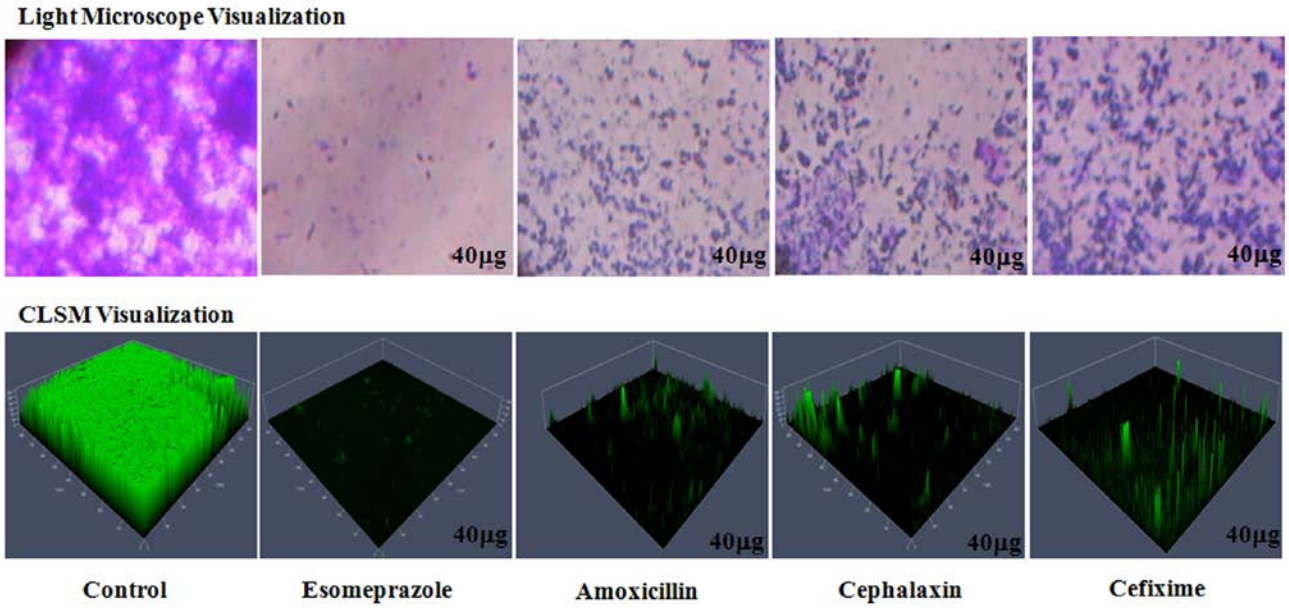

Figure 9

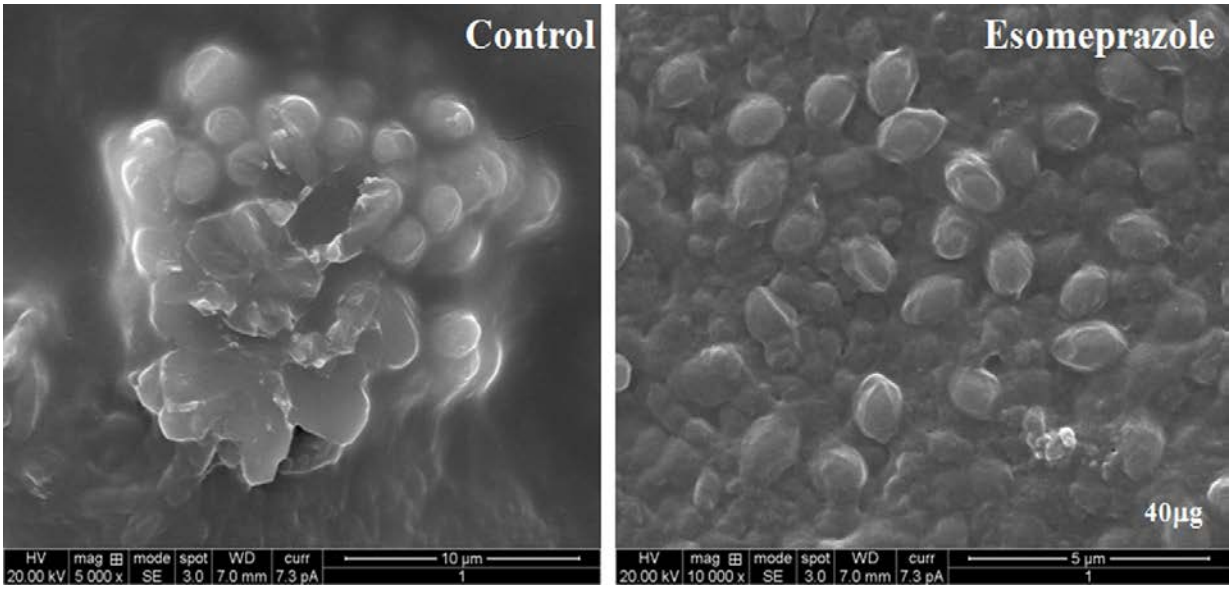

Figure 10a

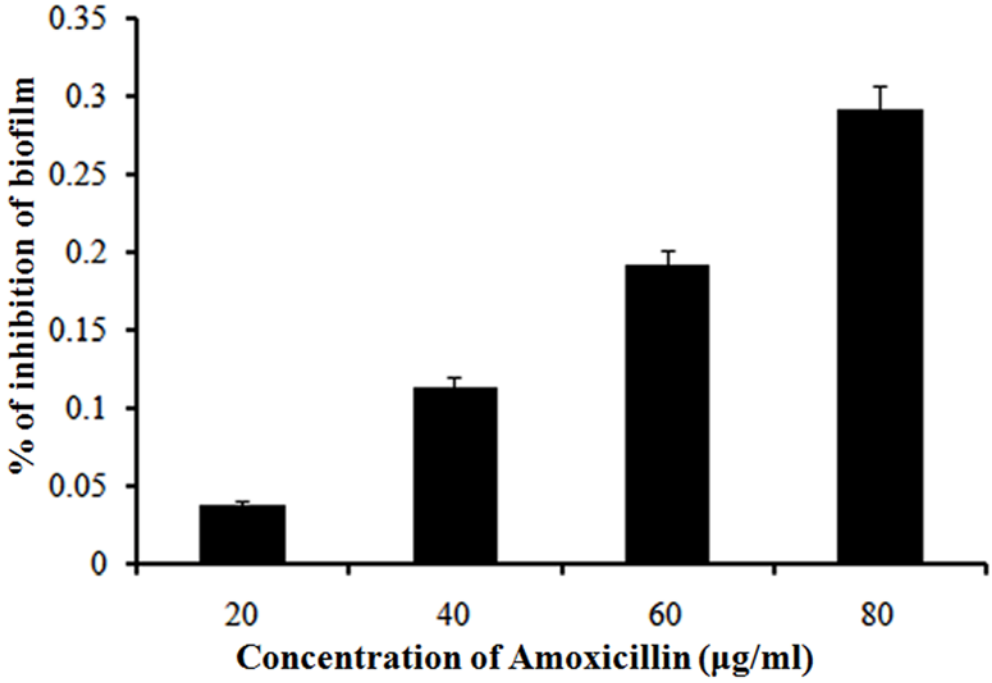

Figure 10b